15TH IEA HEAT PUMP CONFERENCE
MAY 26–29, 2026 | HOFBURG
VIENNA 2026
DECARBONISATION THROUGH INNOVATION

Numerical Modeling of Permafrost Freeze–Thaw Dynamics Using a Finite-Element Framework

M. Ahmadfard, I. Ghalayini, S. B. Dworkin*

Department of Mechanical, Industrial, and Mechatronics Engineering, Toronto Metropolitan University, 350 Victoria St., Toronto, Ontario M5B 2K3, Canada

Abstract

Permafrost thaw driven by ongoing climate warming poses significant risks to infrastructure in cold-region and high-latitude environments, particularly in remote subarctic communities where ground stability is essential for building safety. To improve understanding of ground thermal behavior and support future decarbonization strategies involving ground heat transfer, this study develops and validates a numerical model of permafrost using COMSOL Multiphysics. The model simulates transient heat transfer with phase change to capture the thermal response of fully saturated, ice-rich soils representative of subarctic conditions. Model validation is performed using a two-layer soil profile consisting of an upper organic peat layer overlying mineral soil and subjected to realistic seasonal surface-temperature forcing. Three scenarios of increasing complexity are used to assess the model's accuracy and applicability. Although the physical problem is inherently three-dimensional, the assumptions adopted in this study reduce the thermal response to a predominantly one-dimensional vertical process. For clarity and improved visualization of freeze–thaw transitions, the governing equations and simulation results are presented in a two-dimensional form. The results reproduce characteristic freeze–thaw cycles and demonstrate the buffering effect of latent heat on permafrost temperature evolution. The validated model establishes a foundation for future investigations of engineered systems—such as geo-piles integrated with ground-source heat pumps (GSHPs)—that can both stabilize permafrost and support low-carbon building heating and cooling. Although such integrations lie beyond the present scope, the modeling framework developed here provides a transferable basis for coupled thermal–structural analyses in permafrost regions.

Keywords: Permafrost Thaw; Soil Phase Change; Subarctic Infrastructure Stability; COMSOL Multiphysics; Finite Element Modeling.

1. Introduction

Permafrost is a thermal condition of the ground in which temperatures remain at or below 0 °C for at least two consecutive years [1]. This condition occurs extensively in high-latitude and high-altitude regions, particularly in Arctic and subarctic environments, where it plays a critical role in supporting infrastructure, storing large volumes of ground ice, and regulating hydrological and ecological processes. However, rising air temperatures associated with climate change are causing widespread permafrost warming and thaw, thereby reducing soil strength and threatening the stability of buildings, roads, pipelines, and other infrastructure in cold regions [2].

In permafrost regions, the subsurface typically consists of an active layer that undergoes seasonal thawing and refreezing, underlain by perennially frozen ground and deeper unfrozen material. The thickness of the active layer may range from several tens of centimeters to several meters, while the perennially frozen layer may extend from a few meters to more than one kilometer depending on soil composition, climate, and geothermal heat flux [3]. When ice-rich soils thaw, the loss of ice bonding leads to settlement and ground

*Corresponding author. Tel.: +1-416-979-5000 ex557311
*E-mail address:*seth.dworkin@torontomu.ca

deformation. Among the various forms of settlement that can affect infrastructure, differential settlement—where thaw occurs unevenly beneath a foundation and causes some areas to settle more than others—is particularly problematic, as it can result in tilting, distortion, and loss of structural integrity.

These effects are especially pronounced in remote northern communities, where construction and maintenance are costly and access to replacement materials and technical services is limited. The severity of thaw-induced settlement depends strongly on ground-ice content and cryostructure; soils containing segregated or massive ice can undergo substantial volume loss upon thaw, resulting in pronounced surface subsidence. Continued deepening of the active layer may eventually lead to the formation of taliks—perennially unfrozen zones that persist year-round—which alter subsurface hydrological pathways, reduce seasonal refreezing potential, and accelerate long-term permafrost degradation.

To ensure long-term foundation stability in these environments, it is necessary to understand and predict permafrost thermal response under changing climatic and surface conditions. Numerical modeling provides an effective approach for simulating heat transfer and phase change in frozen soils, allowing for the evaluation of thaw depth evolution and its sensitivity to environmental and soil parameters.

The objective of this study is to simulate the thermal behavior and thaw dynamics of permafrost using a finite-element modeling framework in COMSOL Multiphysics. This modeling framework serves as a foundational step toward future analyses of geo-pile and GSHP systems aimed at foundation stabilization and the decarbonization of building heating and cooling in permafrost-affected regions [4]. The model incorporates transient heat conduction with phase change, representing latent heat effects during the ice–water transition. Because the pore water is assumed to remain immobile, heat transfer occurs solely by conduction, and no groundwater flow or advective heat transport is considered.

This paper is organized as follows. Section 2 reviews current understanding of permafrost thermal processes and numerical modeling approaches. Section 3 presents the governing equations and the associated boundary and initial conditions describing heat transfer with phase change in frozen soils. Section 4 describes the simulation domain, material properties, and the boundary and initial conditions used in this study, selected to represent subarctic ground conditions relevant to the problem. Section 5 presents the simulation results and discusses the factors controlling thaw progression, while Section 6 summarizes the key conclusions.

2. Background and Related Work

The temperature and extent of permafrost are governed by the balance between heat exchange at the ground surface and the upward geothermal heat flux from deeper subsurface layers. Although geothermal heat flux is relatively small (approximately 0.05 W m^{-2}), surface heat fluxes are considerably larger and vary seasonally due to changes in solar radiation, snow cover, vegetation, and soil moisture conditions [5]. These interactions produce a characteristic ground temperature profile in which seasonal temperature fluctuations decrease with depth and eventually vanish at the depth of zero annual amplitude [1]. This is illustrated in Fig. 1, which shows the annual mean, maximum, and minimum temperature profiles and the depth of zero annual amplitude.

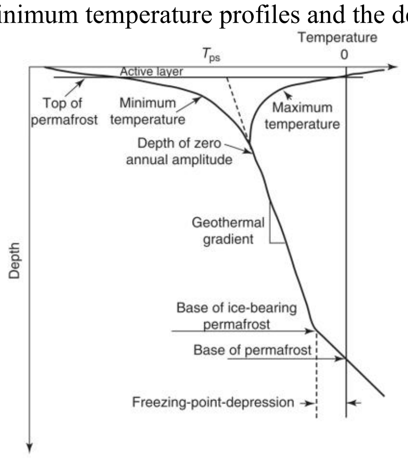

Figure 1. Schematic annual temperature profile in permafrost-affected soil, showing mean, maximum, and minimum temperature curves, active-layer depth, and depth of zero annual amplitude (adapted from [1]).

Permafrost distribution is strongly climate-dependent; however, air temperature alone is not a sufficient predictor because snow and vegetation act as insulating layers that modulate ground heat exchange. The temperature at the top of the permafrost has therefore been used as a more reliable indicator, as it reflects the thermal properties of frozen and unfrozen soil and the influence of surface insulation [6]. Permafrost is commonly classified into continuous (>90% area), discontinuous (50–90%), and sporadic (10–50%) zones [5], and is most widespread in northern continental interiors and cold mountain regions [7].

Recent decades have seen widespread permafrost warming and thaw driven primarily by anthropogenic climate change. The Intergovernmental Panel on Climate Change (IPCC) reports high confidence that permafrost temperatures will continue to rise [8]. Thaw has both environmental and structural consequences: carbon stored in frozen peatlands may be released as greenhouse gases [9], while the loss of ice bonding reduces soil strength, causing settlement and infrastructure damage. By 2050, roughly one-third of pan-Arctic infrastructure may be at risk [10]. This warming causes active-layer thickening; however, the degree of thickening varies regionally due to differences in snow accumulation, vegetation cover, and topographic conditions [11], [12].

Efforts to observe permafrost conditions directly are limited by the remoteness and scale of Arctic terrain, resulting in sparse measurement networks. However, the expansion of the Global Terrestrial Network for Permafrost (GTN-P) has improved the availability of ground-temperature and thaw-depth data [13]. Global climate models also attempt to represent permafrost within coupled land-atmosphere systems; however, the Coupled Model Intercomparison Project (CMIP5 and CMIP6) multi-model ensembles exhibit substantial uncertainties in projecting future thaw extent due to underrepresentation of soil freezing processes, incomplete snow-insulation treatment, and coarse soil depth resolution [11]. This highlights the need for detailed, process-based numerical modeling at local to regional scales.

Numerical heat-transfer models have played a central role in understanding permafrost behavior. Among them, one-dimensional finite-element (FE) models are widely used to simulate vertical temperature evolution and freeze–thaw cycles because of their computational efficiency and suitability for long-term, climate-driven simulations. However, when lateral heat transfer, water migration, engineered foundation systems, or spatially heterogeneous ground conditions are involved, two- or three-dimensional FE models become necessary. Software such as COMSOL Multiphysics enables simulation of heat transfer in soil with phase-change effects, spatially variable geometries, and optional coupling with hydrological processes. COMSOL's ability to capture latent-heat absorption and release during freezing and thawing has been validated [14] against benchmark problems such as the InterFrost T1 test case [15], which compares numerical results against the classical Lunardini analytical phase-change solution [16] as formulated and presented by McKenzie et al. [17].

A central factor in permafrost modeling is the behavior of water during phase change. Freezing in soils occurs over a temperature interval rather than at a single point due to adsorbed unfrozen water films on mineral surfaces [18]. The associated latent-heat release produces the zero-curtain effect, and the higher thermal conductivity of ice compared to liquid water significantly alters subsurface heat transfer [19]. Groundwater flow can also influence thaw progression; in permeable soils, open taliks, or regions with strong hydraulic gradients, advective heat transport may accelerate active-layer deepening and thaw-front migration [20], [21]. However, in many continuous-permafrost settings where soil permeability is low or thaw depths remain shallow, heat transfer is dominated by conduction and advective contributions are limited [22]. Therefore, it is essential to specify whether groundwater flow is included in the modeling framework, because its influence can shift thaw behavior from predominantly conductive to strongly advective regimes.

In the literature, although numerous studies have documented permafrost warming [23], active-layer thickening, and associated infrastructure risks [2], comparatively few have developed numerical models that explicitly and transparently resolve freeze–thaw processes under realistic seasonal boundary conditions [14], [24]. Much of the existing work emphasizes observational trends or passive stabilization measures, such as thermosyphons and crushed-rock embankments, whereas process-based modeling studies often provide limited detail regarding the treatment of latent-heat storage, temperature-dependent unfrozen water content, and phase-change parameterization—making results difficult to reproduce or extend.

Ground-coupled heat-exchange systems have also been implemented in cold regions, including borehole thermal energy storage (BTES) systems designed to reduce fossil-fuel heating demand and GSHP evaluated in partially frozen soils [25], [26]. However, these studies focus primarily on energy supply and system efficiency rather than intentional regulation of ground thermal conditions to limit thaw. Consequently, the potential for actively managing permafrost temperatures through targeted subsurface heat extraction as a means of preventing thaw-induced ground instability remains insufficiently explored.

In this context, there is a need for a transparent and well-documented numerical modeling framework capable of simulating permafrost thermal evolution under seasonal atmospheric forcing, with explicit representation of phase change and temperature-dependent soil properties. The present work develops such a finite-element model and demonstrates its ability to reproduce characteristic freeze–thaw behavior, including freezing-front migration and the zero-curtain effect. This modeling framework provides a physically consistent basis for assessing thaw sensitivity in subarctic soils and will support future investigations into engineered foundation systems that actively interact with ground thermal regimes, including geo-piles [4], which function as both structural supports and ground heat exchangers. While the evaluation of such stabilization strategies is not undertaken here, the model developed in this study is constructed to enable their analysis. Beyond geotechnical stability, such coupled thermal–structural models also support the design of sustainable energy systems in cold regions. When extended to simulate GSHP operation, the same modeling framework can quantify how subsurface heat extraction contributes to both permafrost preservation and decarbonization of building heating and cooling. This establishes the present work as a foundational step linking permafrost modeling with low-carbon thermal energy technologies.

3. Governing Equations and Physical Model

Heat transfer in frozen ground involves the combined effects of heat conduction through the soil matrix, latent heat exchange during phase change of pore water, and external thermal forcing from the atmosphere and underlying earth. In the most general form, the transient heat-transfer equation in porous media includes conductive and advective transport, internal heat generation, and viscous dissipation. However, in permafrost soils, advective heat transport associated with groundwater flow is typically negligible because the hydraulic conductivity of frozen or partially frozen soils is extremely low and fluid movement is strongly restricted [27]. Viscous dissipation and internal heat sources are likewise negligible at the spatial and temporal scales considered. The solid mineral skeleton and pore water/ice are treated as effectively incompressible, and no shear-driven flow occurs; thus, pressure–work and viscous dissipation terms are omitted from the energy balance. Consequently, heat transfer is assumed to occur solely by conduction, and groundwater flow, advective heat transport, and vapor transport are considered negligible under the frozen and partially frozen conditions examined. The thermal effect of freezing and thawing is incorporated through an apparent heat-capacity representation of latent heat.

Heat transfer with phase change in frozen soils may be formulated in one-, two-, or three-dimensional domains depending on the problem geometry and the variability of thermal boundary conditions. In this study, a one-dimensional vertical soil column is first simulated in COMSOL to validate the numerical implementation, followed by a two-dimensional cross-sectional model used to examine thaw progression under realistic seasonal forcing. Although the simulations are performed in a two-dimensional domain, the adopted assumptions result in a predominantly one-dimensional thermal response. Nevertheless, the governing equations are kept in their two-dimensional form to maintain generality and to facilitate clearer visualization of freeze–thaw behavior.

The soil domain is modeled as a two-dimensional, homogeneous, fully saturated porous medium occupying a region $\Omega \subset \mathbb{R}^2$ with horizontal coordinate x and vertical coordinate z, where z is positive upward. The ground surface corresponds to $z = 0$, and depth below ground is represented by negative z values. Temperature is therefore expressed as $T(x, z, t)$ in space and time. The porous medium consists of a solid mineral matrix, liquid water, and ice. The soil is modeled as fully saturated $(S = 1)$, such that the pore space is entirely occupied by liquid water and/or ice. Any pore air that may exist in reality is neglected and does not contribute to heat storage or conduction. In this work, "soil freezing" refers exclusively to the phase change of pore water to ice, while the mineral matrix does not undergo any phase transition. As a result, freezing and thawing influence thermal behavior through temperature-dependent changes in effective volumetric heat capacity and thermal conductivity, while the mineral matrix remains thermally stable and does not contribute to latent heat storage.

The upper boundary Γ_s coincides with the ground surface at $z = 0$, and the lower boundary Γ_b is located at $z = H$. Processes at the ground surface, including snow cover, vegetation shading, and radiative exchange, are not modeled explicitly; instead, their combined influence is represented by prescribing a time-varying surface temperature $T_s(t)$ on Γ_s. At the lower boundary Γ_b, a constant geothermal heat flux q_b is applied to represent upward conductive heat transfer from deeper subsurface layers.

Under these assumptions, conservation of thermal energy in the soil is expressed by the two-dimensional transient heat conduction equation:

$$C_{app}(x, z, T)\frac{\partial T}{\partial t} = \nabla \cdot \left(k_{eff}(x, z, T)\, \nabla T\right), \qquad (x, z) \in \Omega,\ t > 0 \tag{1}$$

where $\nabla = (\partial/\partial x, \partial/\partial z)$ denotes the spatial gradient operator in two dimensions. C_{app} is the apparent volumetric heat capacity [15], [16], [28] and k_{eff} is the scalar effective thermal conductivity, both of which vary with temperature due to the freeze–thaw transition of pore water.

The corresponding one-dimensional form used for validation is obtained by assuming no lateral temperature variation, i.e., $\partial T/\partial x = 0$. Under this assumption, Eq. (1) reduces to:

$$C_{app}(z,T)\frac{\partial T}{\partial t} = \frac{\partial}{\partial z}\left(k_{eff}(z,T)\ \frac{\partial T}{\partial z}\right), \qquad t > 0 \tag{2}$$

The soil is represented as a fully saturated porous medium with porosity ϕ. Because the pores are entirely filled with liquid water and/or ice, the temperature-dependent pore-volume fractions satisfy:

$$\theta_w(T) + \theta_i(T) = \phi \tag{3}$$

Freezing is represented using a temperature-dependent phase-progress function $\alpha(T)$, which varies smoothly from $\alpha = 0$ (fully unfrozen) to $\alpha = 1$ (fully frozen). In this study, no residual unfrozen water is assumed to persist at subfreezing temperatures (i.e., S_{wr}=0), so the volumetric fractions of liquid water and ice reduce to:

$$\theta_w(T) = \phi\big[S_{wr} + (1 - S_{wr})\big(1 - \alpha(T)\big)\big] = \phi[1 - \alpha(T)], \qquad \theta_i(T) = \phi - \theta_w(T) = \phi\alpha(T) \tag{4}$$

A phase change interval of finite width is introduced to represent the gradual freezing of pore water. Conceptually, the phase-progress function may be written as a linear transition across a mushy zone of width ΔT_{m} centered on the nominal freezing temperature T_f:

$$\alpha(T) = \begin{cases} 1. & T \le T_f - \Delta T_m/2\,, \\ \left(T_f + \Delta T_m/2 - T\right)/\Delta T_m, & T_f - \Delta T_m/2 < T < T_f + \Delta T_m/2\,, \\ 0, & T \ge T_f + \Delta T_m/2 \end{cases} \tag{5}$$

with corresponding derivative:

$$\frac{d\alpha}{dT} = \begin{cases} 0, & T \le T_f - \Delta T_m/2\,, \\ -1/\Delta T_m, & T_f - \Delta T_m/2 < T < T_f + \Delta T_m/2\,, \\ 0, & T \ge T_f + \Delta T_m/2 \end{cases} \tag{6}$$

Here, ΔT_{m} denotes the finite temperature interval over which phase change occurs and should not be confused with temperature differences that drive conductive heat transfer. In practice, sharp corners in Eqs. (5)–(6) can introduce numerical stiffness near the freeze–thaw front. Therefore, in COMSOL the phase-progress function is implemented as a smoothed transition using the built-in flc2hs function, $\alpha(T) = flc2hs(T - T_f, \varepsilon_T)$, where ε_T controls the smoothing width and is chosen such that the effective transition region matches ΔT_m. This preserves the total latent heat while providing improved convergence and stability during phase change. This smoothed form is used in the present work, ensuring a continuous and differentiable $d\alpha/dT$ profile and stable numerical performance while maintaining the same physical representation of latent heat as the conceptual piecewise-linear model.

The volumetric heat capacity excluding latent heat is expressed as a volume average of the solid matrix, liquid water, and ice contributions:

$$C_{sens}(T) = (1 - \phi)\rho_s c_s + \theta_i(T)\rho_i c_i + \theta_w(T)\rho_w c_w \tag{7}$$

Similarly, the effective thermal conductivity is

$$k_{eff}(T) = (1 - \phi)k_s + \theta_i(T)k_i + \theta_w(T)k_w \tag{8}$$

The corresponding bulk density of the soil–water–ice mixture is:

$$\rho_{bulk}(T) = (1 - \phi)\rho_s + \theta_i(T)\rho_i + \theta_w(T)\rho_w \tag{9}$$

Here, $\rho_{bulk}(T)$ is the mixture density per unit bulk volume; it varies with temperature through θ_w and θ_i. During freezing and thawing, the internal energy of the pore water changes due not only to temperature variation (sensible heat), but also due to the phase transition between liquid water and ice. The contribution of the phase change is represented using the apparent heat-capacity method, in which the latent heat of fusion L is embedded through the temperature-dependent liquid water fraction $\theta_w(T)$. Because only the liquid water phase undergoes freezing and thawing, the latent heat term is expressed using the density of liquid water ρ_w rather than the bulk mixture density.

The apparent volumetric heat capacity is written as:

$$C_{app}(T) = C_{sens}(T) + \rho_w L \frac{d\theta_w(T)}{dT} = C_{sens}(T) - \rho_w L\phi \frac{d\alpha(T)}{dT} \tag{10}$$

Because $\alpha(T)$ represents the ice phase fraction, $d\alpha/dT$ is negative within the mushy zone, and the minus sign in Eq. (10) ensures a positive latent-heat contribution during thawing. This formulation introduces the latent heat effect directly into the heat-capacity term, allowing phase change to be captured implicitly without explicitly tracking the freezing/thawing interface, thereby avoiding the need for Stefan-type moving-boundary formulations and ensuring numerical stability. The apparent heat capacity used in Eq. (1) is expressed by Eq. (10).

The thermal model requires specification of boundary conditions at the ground surface, the lower boundary, and the lateral boundaries of the domain, in addition to an initial temperature field. At the ground surface ($z = 0$), the temperature is prescribed as a function of time:

$$T(x, 0, t) = T_s(t) \tag{11}$$

where $T_s(t)$ is the externally imposed ground-surface temperature. This condition implicitly accounts for the combined effects of snow cover, vegetation shading, atmospheric exchange, and radiative forcing, without representing these processes explicitly.

At the bottom boundary $(z = -H)$, the thermal interaction with deeper subsurface layers can be represented using either a prescribed geothermal heat flux or an equivalent temperature condition. In the standard formulation, an upward geothermal heat flux $q_b > 0$ (W m^{-2}) is applied. Because the vertical coordinate increases upward, this flux acts in the positive z-direction. With the outward unit normal at the lower boundary given by $\boldsymbol{n} = (0, -1)$, the Neumann condition is

$$-\boldsymbol{n} \cdot \left(k_{eff}(x, z, T)\, \nabla T\right)\big|_{z=-H} = -\boldsymbol{q_b} \tag{12.a}$$

Alternatively, the lower boundary may be specified using a temperature consistent with the geothermal gradient,

$$T(x.z = -H.t) = T_0(x.z = -H) + GH + \Delta T_b(t) \tag{12.b}$$

where T_0 is the mean annual surface temperature, G is the geothermal gradient (K m^{-1}), and $\Delta T_b(t)$ is an optional time-dependent temperature offset used to represent long-term climatic warming or other deep-temperature trends. The flux condition (Eq. 12.a) is appropriate when deep temperatures are assumed stable, whereas the temperature condition (Eq. 12.b) is suitable when evaluating scenarios in which the thermal regime at depth evolves over time.

Along the lateral boundaries, the domain is assumed to be thermally insulated, meaning that no heat is exchanged across these boundaries. Denoting the lateral boundary by Γ_l and the outward unit normal by $\boldsymbol{n}$, the adiabatic (no-flux) condition is expressed as:

$$-\boldsymbol{n} \cdot \left(k_{eff}(x, z, T)\, \nabla T\right)\big|_{\Gamma_l} = 0 \tag{13}$$

Finally, the simulation is initialized by prescribing a temperature field at $t = 0$:

$$T(x, z, 0) = T_0(x, z) \tag{14}$$

where $T_0(x, z)$ is typically constructed from measured near-surface temperatures and extended through depth in accordance with the local geothermal gradient.

In many permafrost environments, the subsurface is stratified, consisting of distinct layers of peat, mineral soil, and ice-rich horizons, each with different porosity, ice content, and thermal properties. In such cases, the thermo-physical parameters are commonly assigned piecewise according to depth, and heat conduction may be anisotropic, with thermal conductivity differing in the vertical and horizontal directions due to sedimentary fabric or preferential ice structures. These effects can influence thaw propagation and the spatial pattern of the active layer, especially in heterogeneous or fine-scale stratified soil profiles.

However, in the present study, the subsurface is modeled as homogeneous and isotropic, with uniform porosity and thermal properties throughout the domain. Layering and directional anisotropy are therefore not included, and heat transfer is assumed to occur by scalar thermal conductivity. This approach allows the governing heat-transfer equation presented above to be applied without modification, together with the temperature-dependent constitutive relations defined in Eqs. (3)–(10).

4. Numerical Model Setup

The numerical simulations are conducted in a two-dimensional vertical soil column extending from the ground surface at $z = 0$ m to a depth of $z = -50$ m. The upper 0.6 m represents an organic peat layer, while the underlying portion is modeled as mineral soil. The out-of-plane thickness is set to 1 m, interpreted as a laterally extensive ground mass. A mapped quadrilateral mesh is applied across the domain, with refinement concentrated near the surface and within the active layer to resolve steep temperature gradients and latent-heat effects. Mesh size increases geometrically with depth to maintain computational efficiency. Figure 2 shows the mesh for the upper 5 m of the soil profile, with the interface at $z = -0.6$ m marking the peat–mineral transition. Mesh-independence checks confirmed that further refinement does not alter the simulated thaw depth or temperature profiles, and the solver relative tolerance is set to 1×10^{-4}.

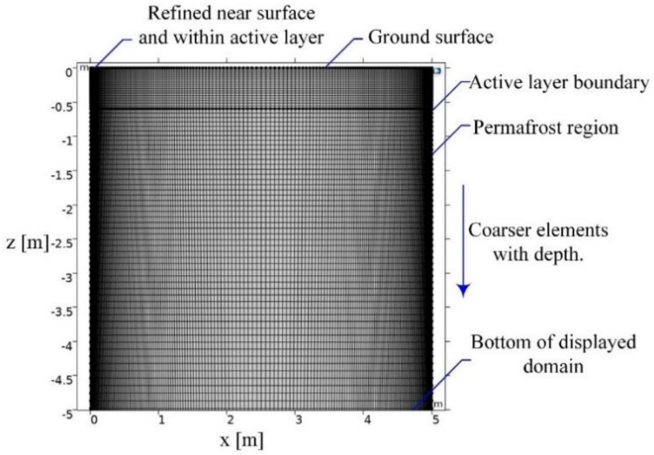

Figure 2. Finite-element mesh of the upper 5 m of the soil column

The soil is assumed fully saturated and isotropic, with heat transfer occurring solely by conduction. Phase change is represented through the apparent heat-capacity method with a mushy-zone width $\Delta T_m = 0.3$ °C and a latent heat of fusion of 3.34×10^5 J kg^{-1}. Table 1 summarizes the thermal and physical properties assigned to the peat and mineral soil layers. Water and ice properties are identical in both layers, with $\rho_w = 1000$ kgm^{-3}, $c_w = 4180$ J kg^{-1} K^{-1}, k_w=0.6 W m^{-1} K^{-1}; $\rho_i = 917$ kg m^{-3}, $c_i = 2100$ J kg^{-1} K^{-1}, and k_i= 2.2 W m^{-1} K^{-1}. The geothermal gradient is set to $G = 0.025$ K m^{-1}, corresponding to a constant upward geothermal heat flux of $q_b = 0.05$ W m^{-2}.

Table 1. Main thermal and physical parameters for peat and mineral soil layers.

Property	Peat Layer (0–0.6 m)	Mineral Soil (> 0.6 m)
Porosity (–)	0.9	0.6
Saturation (–)	1.0	1.0
Solid density (kg m^{-3})	1000	2650
Solid heat capacity (J kg^{-1} K^{-1})	1500	800
Solid thermal conductivity (W m^{-1} K^{-1})	0.75	2.0

The upper boundary temperature follows the harmonic ground-temperature formulation [29] (Eq. 15), which captures the attenuation and phase shift of seasonal thermal waves in the soil.

$$T(z,t) = T_{avg} - \left[T_{amp1}\, exp(-z \cdot \beta_1) \cdot cos\left(\left(\frac{2\pi}{365}\right)(t - P_1) - z \cdot \beta_1\right)\right] - \left[T_{amp2}\, exp(-z \cdot \beta_2) \cdot cos\left(\left(\frac{4\pi}{365}\right)(t - P_2) - z \cdot \beta_2\right)\right] \quad (15)$$

where $\beta_1 = \sqrt{(\pi/(\alpha \cdot 365))}$ and $\beta_2 = \sqrt{(2\pi/(\alpha \cdot 365))}$. The parameters used are $T_{\text{avg}} = -1$ °C, $T_{\text{amp1}} =$ 15 °C, $T_{\text{amp2}} = -3$ °C, $P_1 = 24$ days, $P_2 = 30$ days, and $\alpha = 0.08$ m^2 day^{-1}. These parameters represent typical subarctic conditions, with a mean annual ground temperature of −1 °C and seasonal extremes of roughly −16 °C in winter and +14 °C in summer. The same formulation is used to generate the initial temperature field where needed. Figure 3 shows the resulting temperature variation with depth and time, highlighting the expected seasonal fluctuations and their attenuation and phase lag with depth.

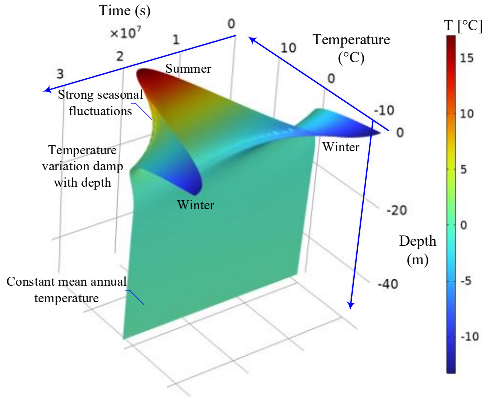

Figure 3. Modelled ground-temperature variation with time and depth.

The lateral boundaries are treated as adiabatic, consistent with the effectively one-dimensional thermal response resulting from laterally uniform forcing and material properties. Two forms of the lower boundary condition are used depending on the scenario: when deep temperatures are assumed stable, a constant geothermal heat flux of q_b= 0.05 W m⁻² is applied; for the long-term warming scenario, the lower boundary is prescribed as a temperature consistent with the geothermal gradient and increased by 0.1 °C per year, implemented as a time-dependent Dirichlet condition at $z = -50$ m.

Three test scenarios of increasing complexity are simulated, differing only in their initial and boundary conditions; all material properties, geometry, and meshing remain identical. In *Scenario 1*, the entire soil column begins at 0 °C, the surface is held at 5 °C, and the lower boundary applies the geothermal flux, providing a baseline transient-thaw test. *Scenario 2* uses the harmonic formulation (Eq. 15) for both the initial condition and the evolving surface temperature, with the geothermal flux again applied at the base, thereby resolving the seasonal freeze–thaw cycle. *Scenario 3* also uses Eq. 15 but adds a long-term climatic warming trend: the mean annual surface temperature increases by 0.1 °C per year, and the lower boundary temperature increases at the same rate. Although real deep-ground temperatures would lag surface warming, this idealized representation isolates the multidecadal effects of sustained warming.

All simulations are performed with the Heat Transfer in Porous Media interface in COMSOL Multiphysics 6.3 using implicit time stepping and adaptive control. Simulations were run on an Intel® Core™ i7-14700F (2.10 GHz) workstation with 32 GB RAM; Scenario 1 required ~1.75 min, Scenario 2 ~2.2 min, and Scenario 3 ~1hr 32 min of wall-clock time. Scenarios 1 and 2 are run for one year, and Scenario 3 for 30 years. The resulting temperature fields are used to evaluate thaw depth, seasonal freeze–thaw dynamics, and the sensitivity of permafrost behavior to boundary-condition complexity.

5. Simulation Results and Discussion

This section presents the results of the three numerical experiments. Phase change is treated using the smoothed apparent heat-capacity method $flc2hs(T - T_f, \varepsilon_T)$ with a transition width of ε_T=ΔT_m=0.3 °C around the freezing temperature T_f = 273.15 K, ensuring latent heat is represented accurately while maintaining numerical stability. The resulting mushy zone, where pore water freezes or thaws gradually, is visualized in all figures using three reference isotherms: the $T = T_f$ contour in yellow, $T = T_f - \Delta T_m = -0.3\,°C$ in cyan, and $T = T_f + \Delta T_m = 0.3\,°$ C in red. Soil between the cyan and red curves is partially frozen, soil colder than the cyan line is fully frozen, and soil warmer than the red line is fully thawed.

Because lateral boundaries are insulated and the domain is horizontally uniform, heat transfer occurs solely by vertical conduction, making the problem effectively one-dimensional; however, for presentation, Scenario 1 is shown in 1-D, while Scenarios 2 and 3 are shown in 2-D for clearer visualization.

5.1. Scenario 1: Transient Thawing Under Constant Surface Warming

Scenario 1 provides a baseline test of the model by applying simple, non-seasonal warming to an initially isothermal soil column. The entire 50-m profile begins at 0 °C, the ground surface is fixed at 5 °C for one year, and the lower boundary imposes the constant geothermal flux of 0.05 W m⁻². With no cooling phases or seasonal variability, heat propagates purely by vertical conduction. Figure 4 shows the one-dimensional temperature–depth profiles after four, eight, and twelve months, focusing on the upper 5 m where thermal gradients are largest.

Because the soil begins uniformly at 0 °C and experiences only warming, temperatures never fall below freezing and the cyan ($T_f - \Delta T_m$ =−0.3 °C) isotherm does not appear. The yellow 0 °C contour steadily moves downward as latent heat is consumed to melt pore ice, while the red ($T_f + \Delta T_m$ =+0.3 °C) isotherm stays near the surface and deepens only slightly, indicating that warming above the melting point is much slower than the advance of the thaw front.

During the first four months, heat penetration is limited by the low thermal diffusivity of the peat layer, which retards the initial descent of the thaw front. As the warming wave reaches the underlying mineral soil—whose diffusivity is roughly twice that of peat—the downward migration of the 0 °C isotherm accelerates, producing the more rapid deepening observed between four and eight months. At greater depths, the advance slows again because less surface energy reaches the thaw front and latent heat must still be supplied before temperatures can rise above freezing. From a theoretical standpoint, a purely conductive step change would yield a characteristic penetration depth $\delta \approx 2\sqrt{\alpha t}$, where $\alpha = k_{eff}/C_{sens}$ is computed from the material properties in Table 1; however, this provides an upper bound because it neglects phase change. In the present case, freezing and thawing are governed by an enthalpy (apparent heat-capacity) formulation, for which the thaw-front depth $s(t)$—defined by the $T = T_f$ (0°C) isotherm—is expected to scale as $\sqrt{\alpha t}$ but with a reduced prefactor controlled by the Stefan number. Using the imposed surface warming ($T_s - T_f$= 5 °C) and the latent heat of fusion, the Stefan number is much less than unity, indicating strong latent-heat buffering. Accordingly, the numerically simulated thaw depth—increasing roughly with $\sqrt{t}$ between 4, 8, and 12 months and reaching approximately 1.5 m after one year—is consistent with diffusion-limited, phase-change-controlled penetration rather than pure conduction.

This evolution reflects the contrasting thermal properties of the two layers. The peat warms readily due to its low conductivity and low volumetric heat capacity, while the mineral soil conducts heat more efficiently but requires more energy to warm because of its higher volumetric heat capacity. These combined effects shape the rate and depth of thaw, confirming that the model reproduces conductive heat transfer, latent-heat buffering, and material-dependent thermal response under simple forcing.

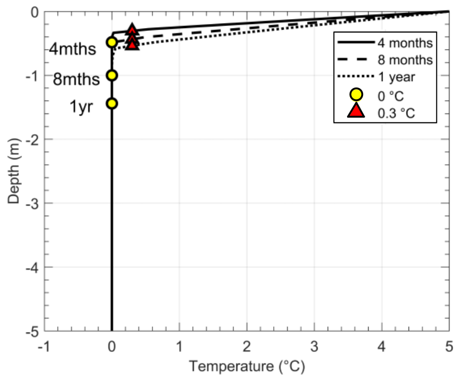

Figure 4. Downward progression of the thaw front in Scenario 1 at 4, 8, and 12 months.

5.2. Scenario 2: Seasonal Freeze–Thaw Cycling

Scenario 2 applies the harmonic ground-temperature forcing (Eq. 15) to both the initial temperature field and the upper boundary, while the lower boundary maintains the constant geothermal flux of 0.05 W m⁻². This produces a full winter–summer cycle characteristic of subarctic soils. Figure 5 shows the resulting one-year temperature evolution.

At the start of the simulation (mid-winter), the upper several meters are strongly frozen, with temperatures decreasing upward from about –0.3 °C at depth to roughly –14 °C at the surface. Beneath this frozen zone lies a shallow layer at slightly positive temperatures, followed by a colder permafrost layer extending from roughly 10 to 40 m depth. The deepest soil warms only gradually toward 0 °C under the geothermal gradient because no prior multi-year warming is imposed.

As surface temperatures rise through spring and summer, the active layer warms and thickens. Energy is first used to raise frozen soil to the melting point and then to supply the latent heat of thawing. The low thermal diffusivity of the peat layer introduces a noticeable lag in its response, while the mineral soil conducts part of the summer heat pulse deeper. By late summer (around day 210), the surface reaches peak temperatures and sends a strong downward heat pulse, visible in Figure 5 as brightening contours. This pulse continues to propagate downward even as the surface begins to cool, producing continued warming of the upper permafrost into early autumn. This delayed response arises from seasonal phase lag within the single simulated year.

During autumn and early winter, the shallow layers cool sharply and refreeze as the surface temperature drops below 0 °C. Deeper layers retain their lagged behavior: the transitional zone cools from its summer maximum but remains slightly above freezing by year-end, while the permafrost warms by a few tenths of a degree relative to its initial state. In Figure 5, this appears as a slight lightening of the permafrost contours late in the year. The modest net warming results from the deeper penetration of the summer heat pulse compared with the winter cold pulse, combined with latent-heat release during refreezing, which reduces the efficiency of winter cooling.

Overall, Scenario 2 reproduces the essential features of seasonal permafrost dynamics: strong surface-driven thermal oscillations, attenuation and phase lag with depth, annual formation and collapse of the active layer, and a lagged warming of the upper permafrost despite winter refreezing.

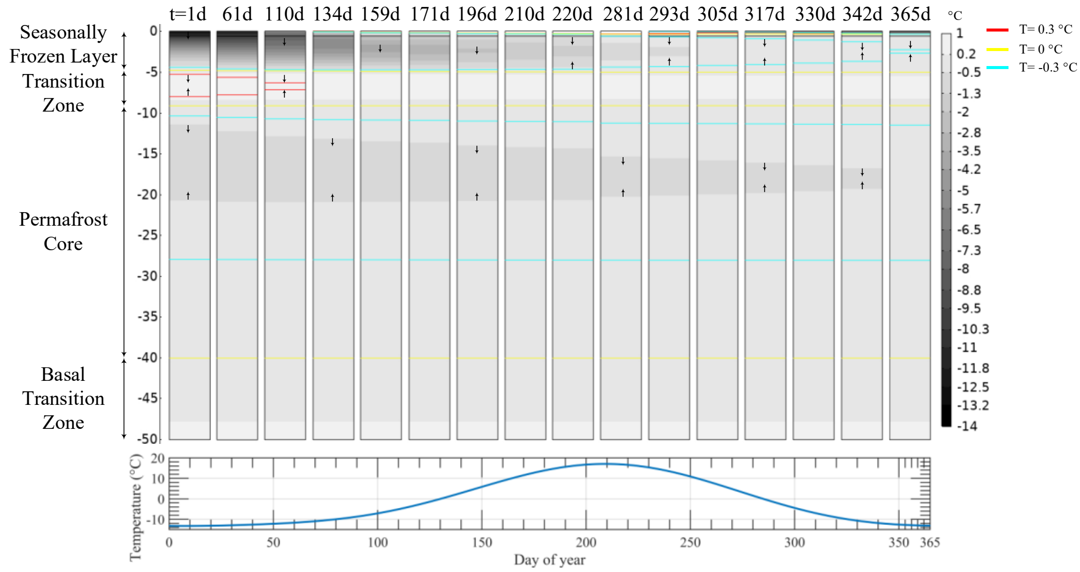

Figure5. Subsurface temperature evolution for Scenario 2 shown at 16 times over one year, capturing seasonal thawing, refreezing, and phase lag. Bottom: imposed harmonic ground-surface temperature boundary condition.

5.3. Scenario 3: Multidecadal Warming Under Increasing Surface and Deep Temperatures

Scenario 3 examines the long-term response of the soil column to sustained climatic warming by increasing the mean annual surface temperature by 0.1 °C yr^{-1} and imposing the same rate of warming at the lower boundary. Although real deep-ground temperatures would lag the surface, this symmetric forcing isolates the cumulative effects of persistent warming from both boundaries.

Figure 6 presents winter temperature profiles (day 1 of each year) at two-year intervals over 30 years. Because all snapshots correspond to mid-winter, the active layer is seasonally frozen in every profile, and long-term changes appear primarily as shifts in winter temperatures rather than changes in thaw depth.

In the upper 1–2 m, the winter cold pulse dominates the relatively small annual warming trend, and the insulating peat layer further delays heat transfer. Consequently, mid-winter surface temperatures appear nearly unchanged across decades. This behavior reflects timing—not cooling—because summer warming is not shown in these winter-only profiles.

Below the active layer, the transitional zone cools slightly in winter due to the same seasonal effects. In contrast, the permafrost steadily warms by several tenths of a degree, evidenced by the gradual upward migration of the +0.3 °C isotherm toward the permafrost table. This long-term warming results from increased conductive heat input at both boundaries and from the fact that summer heat penetrates more efficiently than winter cold, while latent-heat release during refreezing reduces the depth of winter cooling.

Overall, Scenario 3 demonstrates how modest but persistent climatic warming can significantly increase permafrost temperatures over multidecadal timescales. Even though surface layers continue to refreeze each winter, the deeper permafrost accumulates heat due to phase-lagged conduction and the imposed warming trends, indicating a trajectory toward eventual thaw.

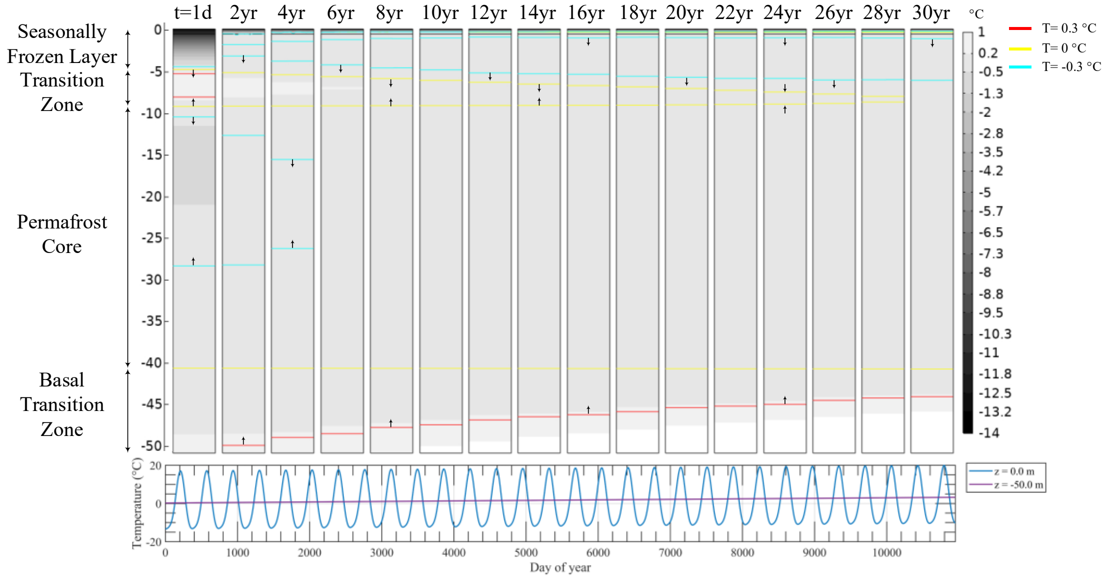

Figure 6. Subsurface temperature evolution for Scenario 3 at 16 times over 30 years, showing progressive permafrost warming under +0.1 °C yr^{-1} surface and basal temperature trends. Bottom: imposed temperature boundary conditions.

6. Conclusions

This study developed and validated a finite-element modeling framework capable of resolving conductive heat transfer and phase change in saturated, ice-rich soils representative of subarctic permafrost. By employing COMSOL's apparent heat-capacity formulation, the model accurately captured key physical processes; freeze–thaw transitions, latent-heat buffering, the zero-curtain effect, active-layer dynamics, and the seasonal attenuation and phase lag of surface thermal forcing. Across three scenarios of increasing complexity, the results reproduced characteristic thaw-front migration patterns and demonstrated progressive warming of deeper permafrost under sustained climatic trends. These outcomes confirm that the framework can reliably simulate permafrost thermal evolution driven by both short-term variability and long-term warming.

Beyond validating freeze–thaw representation, the modeling results highlight the sensitivity of permafrost stability to subtle shifts in heat flux at the ground surface and at depth. The findings reinforce that latent heat moderates short-term temperature fluctuations while simultaneously enabling the long-term accumulation of subsurface heat—an effect that plays a central role in the deepening of the active layer and the onset of talik formation. This underscores the need for engineered interventions capable of managing subsurface thermal regimes in cold-region built environments.

The numerical framework developed here establishes a foundation for such interventions. Because the model explicitly resolves conductive heat exchange and latent-heat consumption, it can be extended to evaluate thermally active foundation systems, including geo-piles, energy piles, and ground-source heat pump (GSHP) integrated foundations. These systems offer dual benefits that directly connect the present work to broader decarbonization goals. First, by extracting heat from the ground during building operation, GSHP-coupled geo-piles can actively cool and preserve ice-rich soils, reducing thaw-related deformation and increasing foundation resilience. Second, by supplying low-carbon heating and cooling to buildings, such systems help reduce reliance on fossil fuels in remote northern communities—where fuel transport costs and emissions are especially high.

Thus, while this paper focuses on fundamental freeze–thaw modeling and validation, it provides the rigorous thermal backbone required for future coupled thermal–structural simulations of permafrost-sensitive foundations. The modeling framework can be readily adapted to quantify how engineered heat extraction strategies influence thaw progression, stabilize permafrost beneath critical infrastructure, and contribute to the long-term decarbonization of northern built environments. Continued development in this direction will enable optimized designs for geo-piles and GSHP systems specifically tailored to cold-region challenges, supporting both infrastructure longevity and sustainable energy transitions.

Acknowledgements

The authors would like to acknowledge Mr. Andrew Lee of Innovia GEO Corp. for his technical advice and expertise, as well as the financial support provided by the Canada Research Chairs Program, the Natural Sciences and Engineering Research Council (NSERC) of Canada, and Innovia GEO Corp.

References

[1] T. Osterkamp and C. Burn, "Permafrost," in *Encyclopedia of Atmospheric Sciences*, J. R. Holton, Ed., Oxford: Academic Press, 2003, pp. 1717–1729.
[2] B. B. Calmels F, Horton B, Roy LP, Lipovsky P, "Assessment of Risk to Infrastructure from Permafrost Degradation and a Changing Climate, Ross River," 2016.
[3] H. M. French, *The Periglacial Environment*, 4th Editio. Chichester, UK: Wiley-Blackwell, 2017.
[4] S. R. Nicholson, "Characterization of a novel in-ground heat exchanger for applications in sustainable building energy and maintaining permafrost," Ryerson University, 2020.
[5] P. J. Williams and M. W. Smith, *The Frozen Earth: Fundamentals of Geocryology - Studies in Polar Research*. Cambridge: Cambridge University Press, 1991.
[6] M. W. Smith and D. W. Riseborough, "Climate and the Limits of Permafrost : A Zonal Analysis," *Permafr. Periglac. Process.*, vol. 13, no. 1, pp. 1–15, 2002.
[7] J. Obu *et al.*, "Earth-Science Reviews Northern Hemisphere permafrost map based on TTOP modelling for 2000 – 2016 at 1 km2 scale," *Earth-Science Rev.*, vol. 193, pp. 299–316, 2019.
[8] M. Meredith *et al.*, *Polar regions. chapter 3, IPCC special report on the ocean and cryosphere in a changing climate*. 2019.
[9] G. Hugelius, J. Loisel, S. Chadburn, R. B. Jackson, M. Jones, and G. Macdonald, "Large stocks of peatland carbon and nitrogen are vulnerable to permafrost thaw," 2020, pp. 20438–20446.
[10] J. Hjort *et al.*, "Degrading permafrost puts Arctic infrastructure at risk by mid-century," *Nat. Commun.*, vol. 9, no. 1, pp. 1–9, 2018.
[11] B. Fox-Kemper *et al.*, "Ocean, Cryosphere and Sea Level Change," in *Climate Change 2021: The Physical Science Basis. Contribution of Working Group I to the Sixth Assessment Report of the Intergovernmental Panel on Climate Change*, V. Masson-Delmotte, P. Zhai, A. Pirani, S. L. Connors, C. Péan, S. Berger, N. Caud, Y. Chen, L. Goldfarb, M. I. Gomis, M. Huang, K. Leitzell, E. Lonnoy, J. B. R. Matthews, T. K. Maycock, T. Waterfield, R. Yelekçi, O., Yu, and B. Zhou, Eds., Cambridge, UK and New York, NY, USA: Cambridge University Press, 2021, pp. 1211–1362.
[12] M. W. Smith and D. W. Riseborough, "Permafrost Monitoring and Detection of Climate Change," *Permafr. Periglac. Process.*, vol. 7, no. 4, pp. 301–309, 1996.
[13] S. L. Smith *et al.*, "Widespread permafrost degradation: Updates from global terrestrial network for permafrost," in *AGU Fall Meeting Abstracts*, 2022, pp. C42E–1069.
[14] V. A. I. Korhonen, "Modelling heat transfer in permafrost with COMSOL," University of Helsinki, 2023.
[15] H. Anbergen, W. Rühaak, J. Frank, and I. Sass, "Numerical simulation of a freeze-thaw testing procedure for borehole heat exchanger grouts," *Can. Geotech. J.*, vol. 52, no. 8, pp. 1087–1100, 2015.
[16] V. J. Lunardini, "Freezing of Soil with an Unfrozen Water Content and Variable Thermal Properties," 1988.
[17] J. M. Mckenzie, C. I. Voss, and D. I. Siegel, "Groundwater flow with energy transport and water – ice phase change: Numerical simulations, benchmarks, and application to freezing in peat bogs," *Adv. Water Resour.*, vol. 30, pp. 966–983, 2007.
[18] D. Hillel, *Fundamentals of soil physics*. New York: Academic Press, 1980.
[19] L. Bronfenbrener, *Modelling heat and mass transfer in freezing porous media*. New York: Nova Science Publishers, 2012.
[20] M. Diak *et al.*, "Permafrost and groundwater interaction : current state and future perspective," *Front. Earth Sci.*, vol. 11, pp. 1–25, 2023.
[21] B. L. Kurylyk, M. Hayashi, W. L. Quinton, J. M. McKenzie, and C. I. Voss, "Influence of vertical and lateral heat transfer on permafrost thaw, peatland landscape transition, and groundwater flow," *Water Resour. Res.*, vol. 52, no. 2, pp. 1286–1305, 2016.
[22] M. S. Ghias, R. Therrien, and J. Molson, "Numerical simulations of coupled groundwater flow and heat transport incorporating freeze / thaw cycles and phase change in a continuous permafrost environment," in *68e Conférence Canadienne de Géotechnique et 7e Conférence Canadienne sur le Pergélisol*, Québec, Québec, 2015.
[23] B. K. Biskaborn, S. L. Smith, and J. Noetzli, "Permafrost is warming at a global scale," *Nat. Commun.*, vol. 10, no. 264, pp. 1–12, 2019.
[24] E. E. Dagher, G. Su, and T. S. Nguyen, "Verification of the Numerical Simulation of Permafrost Using COMSOL Multiphysics ® Software," in *2014 COMSOL Conference in Boston*, 2014, pp. 1–9.
[25] N. Giordano and J. Raymond, "Alternative and sustainable heat production for drinking water needs in a subarctic climate (Nunavik, Canada): Borehole thermal energy storage to reduce fossil fuel dependency in off-grid communities," *Appl. Energy*, vol. 252, 2019.
[26] E. Norouzi, B. Li, L. L. Wang, J. Raymond, A. Gaur, and J. Zou, "Numerical evaluation of ground source heat pumps in a thawing permafrost region," *J. Build. Eng.*, vol. 98, 2024.
[27] O. T. Farouki, *Thermal properties of soils (CRREL Monograph 81–1)*. Hanover, NH, USA: U.S. Army Cold Regions Research and Engineering Laboratory., 1981.
[28] D. Mottaghy and V. Rath, "Latent heat effects in subsurface heat transport modelling and their impact on palaeotemperature reconstructions," *Geophys. J. Int.*, vol. 164, no. 1, pp. 236–245, 2006.
[29] L. U. Xing, "Estimations of undisturbed ground temperatures using numerical and analytical modeling," Oklahoma State University, 2010.